Journal of Catalysis 280 (2011) 96–103

Contents lists available at ScienceDirect

Journal of Catalysis

journal homepage: www.elsevier.com/locate/jcat

Bridging the materials gap between single crystal and supported catalysts using polycrystalline Ni/Pt bimetallic surfaces for cyclohexene hydrogenation

Michael P. Humbert, Alan L. Stottlemyer, Carl A. Menning, Jingguang G. Chen *

Department of Chemical Engineering, Center for Catalytic Science and Technology (CCST), University of Delaware, Newark, DE 19716, USA

ARTICLE INFO

Article history:
Received 10 January 2011
Revised 22 February 2011
Accepted 8 March 2011
Available online 12 April 2011

Keywords:
Platinum
Nickel
Bimetallic surfaces
Polycrystalline
Hydrogenation

ABSTRACT

The current work utilizes the adsorption of hydrogen and the hydrogenation of cyclohexene as probe reactions to bridge the materials gap between single crystal and polycrystalline Ni/Pt bimetallic surfaces. Previous studies on Ni-modified Pt(1 1 1) have identified the formation of a Pt–Ni–Pt(1 1 1) subsurface structure that binds atomic hydrogen and cyclohexene more weakly, leading to a low-temperature hydrogenation pathway not present on either of the parent metal surfaces. In the current work, the Pt–Ni–Pt subsurface structure is prepared by depositing Ni on a polycrystalline Pt foil substrate. The adsorption of hydrogen and hydrogenation of cyclohexene are investigated using surface science experiments and density functional theory (DFT) calculations. The polycrystalline Pt–Ni–Pt subsurface structure shows general similarities to Pt–Ni–Pt(1 1 1) in the low-temperature hydrogenation pathway, demonstrating the validity of using single crystals to predict activity trends for more complex surfaces.

1. Introduction

The ultimate goal in rational design of catalytic materials is to correlate theoretical calculations with catalytic properties of supported catalysts. Density functional theory (DFT) calculations are typically carried out on well-defined structures of single crystal surfaces. On the other hand, an industrially relevant supported catalyst is typically in the form of nanoparticles that contain various low Miller-index facets as well as edge and defect sites. One way to bridge the "materials gap", between model surfaces in DFT calculations and complex structures in supported catalysts, is to compare the reaction pathways on single crystal and polycrystalline surfaces. Results on the single crystal surface provide a direct verification of DFT predictions; studies on the polycrystalline foil account for the presence of different crystal planes and defects typically present in a supported catalyst. In the current study, we will use the hydrogenation of cyclohexene on polycrystalline Ni/Pt bimetallic surfaces to demonstrate the correlation between DFT calculations, surface science measurements on single crystal and polycrystalline substrates, and reactor evaluations over supported catalysts.

It is well established that bimetallic catalysts often show enhanced catalytic properties when compared to those of the corresponding monometallic materials [1–5]. Recent research has combined theoretical and experimental approaches to elucidate the underlying principles that govern the novel catalytic activity of bimetallic systems [4–6]. A great deal of effort has been devoted to investigate the adsorption and reactions of molecules on model bimetallic surfaces under ultra-high vacuum (UHV) conditions [4,7]. One class of materials that has been particularly interesting is monolayer bimetallic surfaces formed by the deposition of one element onto the substrate of another [3,7,8]. Our research group has conducted extensive experimental studies and DFT calculations on Pt(1 1 1) substrates modified by 3d transition metals, with the Ni/Pt(1 1 1) bimetallic surfaces demonstrating some of the most unique chemical properties [9–15].

Modification of Pt(1 1 1) with approximately one monolayer (ML) of Ni at 300 K results in a surface with Ni atoms residing in a pseudomorphic overlayer on top of the Pt(1 1 1) single crystal, which is referred to as Ni–Pt–Pt(1 1 1). The binding of atomic hydrogen, cyclohexene, and several other adsorbates is stronger on this surface than on Pt(1 1 1) and Ni(1 1 1) [13], which makes it very active toward decomposition and reforming reactions [3,11]. If the Ni–Pt–Pt(1 1 1) surface is heated to 600 K, the surface Ni atoms diffuse into the subsurface layer to form a subsurface Pt–Ni–Pt(1 1 1) structure [13]. The electronic properties of this surface are modified in such a way that it interacts more weakly with adsorbates than Pt(1 1 1) and Ni(1 1 1) [3], with the weak binding energies of atomic hydrogen and unsaturated hydrocarbons leading to several low temperature C=C and C=O hydrogenation reactions [12–15].

In a supported Pt catalyst, the active metal will be present in the form of nanoparticles to maximize utilization of the expensive precious metal. Pt nanoparticles are comprised of not only the

* Corresponding author. Fax: +1 302 831 2085.
E-mail address: jgchen@udel.edu (J.G. Chen).

0021-9517/$ - see front matter © 2011 Elsevier Inc. All rights reserved.
doi:10.1016/j.jcat.2011.03.007

low energy (1 1 1) facets, but also other crystalline facets and an array of edge and defect sites. To account for these additional surface sites, a polycrystalline Pt foil substrate is used in the current study to approximate the morphology of supported Pt and to bridge the materials gap between a Pt(1 1 1) single crystal and more realistic catalytic materials. The hydrogenation of cyclohexene has previously been used as a probe reaction to determine the novel properties of the Ni/Pt(1 1 1) bimetallic system. The hydrogenation pathway is present only on the Pt–Ni–Pt(1 1 1) subsurface structure, due to the weaker bonding of atomic hydrogen and cyclohexene on this surface [9,14]. The main objective of the current study is to determine whether the unique hydrogenation pathway is also present on the corresponding polycrystalline Ni/Pt surfaces, using a combination of surface science experiments and DFT calculations. Specifically, the experiments focus on the identification of surface intermediates and gas-phase products following the reaction of cyclohexene with co-adsorbed hydrogen on Ni/Pt polycrystalline surfaces. The DFT results extend previous Ni/Pt(1 1 1) calculations to Pt(1 0 0) and Ni/Pt(1 0 0). These calculations reflect that both the (1 1 1) and (1 0 0) surface facets are present on the polycrystalline Pt foil, as reported previously [16,17].

2. Experimental and theoretical methods

2.1. Preparation of bimetallic surfaces

The current study utilized two UHV chambers to conduct TPD and HREELS experiments. The TPD experiments were performed in a two-level UHV chamber equipped with an Auger electron spectrometer (AES) for surface characterization and a UTI 100C quadrupole mass spectrometer (MS) for TPD and *in situ* verification of the purity of the dosed gases. The HREELS chamber was equipped with AES, MS, and an LK3000 HREEL spectrometer.

For both chambers, the substrate studied was a polycrystalline Pt foil. The TPD experiments were performed on a 0.5 mm thick foil, which was cut to a diameter of approximately 11 mm. The HREELS experiments used a 0.1 mm thick foil that was cut into a square shape ($\sim$10 mm $\times$ 10 mm) to facilitate tuning of the electron beam. Both foils were purchased from Alfa Aesar and were 99.997% pure. The substrates were each held in place by two tantalum posts. Temperature was measured with a K-type thermocouple, spot-welded to the back of the Pt foil. Temperature control was achieved via resistive heating and nitrogen cooling through the tantalum posts and use of a feedback controller. In this manner, the temperature could be controlled in the range of 100–1100 K.

The Pt foil was cleaned by sputtering with Ne^+ at 600 K. The surface was then exposed to oxygen at 900 K to remove excess carbon, followed by annealing at 1050 K for 300 s. This procedure was repeated until surface cleanliness was verified with AES. The polycrystalline Pt foil in the current study was characterized using glancing incidence X-ray diffraction (GIXRD) [16]. The two dominant peaks were (1 1 1) and (1 0 0) planes, with the latter being detected as (2 0 0) due to the XRD selection rule. Although it is difficult to quantify the surface fractions of different planes from the GIXRD measurements, the detection of (1 1 1) and (1 0 0) as the dominant diffraction peaks suggests that both planes are present on the Pt foil. The presence of both Pt(1 1 1) and Pt(1 0 0) facets on a polycrystalline foil was also reported by McMillan et al. using photoemission electron microscopy (PEEM) [17].

Ni was deposited onto the clean Pt foil at 300 K until the AES peak-to-peak ratio of the Ni (849 eV) to Pt (241 eV) peaks was approximately 1.7. This ratio is representative of approximately one monolayer (ML) of Ni residing on top of the Pt substrate, as determined by standard substrate/overlayer calculations as described in detail elsewhere [14,18]. The surface configuration is referred to as Ni–Pt–Pt foil. To drive Ni into the subsurface region of the Pt substrate, the Ni–Pt–Pt foil was flashed to 725 K and held at that temperature for 30 s, which resulted in the Ni (849 eV)/Pt (241 eV) AES ratio decreasing to approximately 1.0, corresponding to a Pt–Ni–Pt subsurface structure [19].

2.2. TPD measurements

TPD studies were conducted after the adsorption of hydrogen (Matheson, 99.999%), which was dosed into the chamber with the substrate temperature at or below 140 K. Saturation coverage of atomic hydrogen on Pt foil was determined to occur with an exposure of approximately 10 L (1×10^{-7} Torr for 100 s). For the cyclohexene hydrogenation experiments, hydrogen was dosed onto the surface to achieve partial saturation (1 L) followed by a 5 L exposure of cyclohexene (Aldrich, 99+%), which was a high enough exposure to result in multilayer desorption being detected in the TPD spectra. Cyclohexene was purified by successive freeze–pump–thaw cycles prior to use. The TPD measurements were taken with a linear heating rate of 3 K/s.

2.3. HREELS measurements

HREELS spectra were recorded with a primary beam energy of 6 eV. The angles of incidence and reflection of the beam were 60° with respect to the surface normal. Typical count rates were about 10^4 counts per second with spectral resolution of about 55 cm^{-1} full width at half maximum (FWHM). The relatively poor resolution is attributed to the polycrystalline nature of the surfaces. Once the desired surface was prepared and the substrate temperature cooled to below 120 K, the surface was exposed to hydrogen to achieve partial saturation, followed by an exposure of cyclohexene to near monolayer coverage. The adsorbed layer was then flashed to the temperature of interest, at a linear heating rate of 3 K/s, and allowed to cool back down to below 120 K before acquiring the HREEL spectrum.

3. DFT calculations

The binding energies of hydrogen and cyclohexene on Pt(1 0 0), Pt(1 1 1), both with and without ML Ni, were calculated using the Vienna Ab-initio Simulations Package (VASP). All calculations used a $3 \times 3 \times 1$ Monkhorst–Pack k-point mesh and the PW91 functional with a planewave cutoff energy of 396 eV and implemented spin polarization. The Pt(1 1 1) and Pt(1 0 0) surfaces were modeled using a periodic 3×3 unit cell slab with four layers of metal atoms and at least seven equivalent layers of vacuum separated each metal slab. One adsorbate was placed on the surface per unit cell, corresponding to 1/9 ML surface coverage. For the Ni–Pt–Pt surface configuration, the Pt in the top layer was substituted by Ni atoms, while for the Pt–Ni–Pt subsurface configuration Ni atoms replaced Pt in the second atomic layer. During energy minimization, the adsorbate and the top two layers of the metal slab were allowed to relax while the bottom two layers remained frozen at the bulk Pt–Pt distance of 2.83 Å, as previously determined for the PW-91 exchange–correlation functional [3].

The hydrogen binding energy (HBE) and cyclohexene binding energy were calculated, and the results are summarized in Table 1. The binding of cyclohexene was calculated as di-σ-bonded at two adjacent atop sites and in the boat configuration, which was the lowest energy configuration of this molecule. The binding energy values in Table 1 were calculated by subtracting the sum of the total energy of the gas-phase adsorbate and the bare slab from the adsorbate-slab total energy. Since the energy from H–H

Table 1
DFT results of binding energies of atomic hydrogen and cyclohexene.

	0.11 ML (3 × 3 slab) H binding energy (kJ/mol)		0.11 ML (3 × 3 slab) Cyclohexene binding energy (kJ/mol)
	FCC	HCP	
PtNiPt(1 1 1)	−242.6	−239.4	−16.1
NiPtPt(1 1 1)	−289.1	−283.7	−73.8
Pt(1 1 1)	−264.8	−257.6	−66.0
Ni(1 1 1)	−269.4	−268.5	
	4-Fold	Bridge	
PtNiPt(1 0 0)	−271.7	−271.7	−31.5
NiPtPt(1 0 0)	−239.0	−259.6	−43.9
Pt(1 0 0)	−278.7	−278.8	−107.0
Ni(1 0 0)	−264.2	−256.6	

interactions on the surface is generally very small compared with H–M interactions, it was not considered in the calculation of HBE [20].

4. Results and discussion

4.1. DFT calculations of binding energies

As the surface of Pt foil is comprised of a multitude of crystal facets, it is important to first review the behavior of hydrogen adsorption on several low-index Pt single crystals. While hydrogen desorption from Pt surfaces has been studied extensively, it lacks a straightforward interpretation due to reports of multiple binding sites, activation barriers for desorption varying by a factor of two, pre-exponential factors varying over several orders of magnitude, and even disagreement over the order of desorption [13,21–25]. For example, the heat of adsorption of hydrogen on Pt(1 1 1) has been reported to be anywhere from 42 to 90 kJ/mol, with the large discrepancies in literature likely being attributed to step edges and defect sites [25]. Thus, it is difficult to agree on an exact value of the binding energy of hydrogen to each Pt facet, especially those facets that can reconstruct, based on results found in literature. There is a general agreement, however, that the dissociative binding energy of hydrogen (HBE) on Pt(1 1 1), Pt(1 0 0), and Pt(1 1 0) is relatively similar [25]. Markovic and Ross report the HBE on Pt(1 1 1) to be on the order of 240–270 kJ/mol, which compares favorably to the value of 265 kJ/mol reported in Table 1. It should be noted that the focus of the current work is to determine how the modification of Pt foil by Ni would affect hydrogen adsorption energy and hydrogenation activity. Thus, the primary objective for the DFT calculations is to identify trends in the values of hydrogen and cyclohexene binding energies among the different surfaces. As the values for HBE calculated in this work are in the range found in literature, it is concluded that the DFT results obtained and summarized in Table 1 are sufficiently accurate for the purposes of identifying trends among the surfaces reported in the current study.

As compared in Table 1, on the (1 1 1) surfaces the FCC threefold site is slightly preferred over the HCP site for the adsorption of atomic hydrogen. On the (1 0 0) surfaces, the bridge-site is preferred over the 4-fold site on Ni–Pt–Pt(1 0 0) while the opposite is observed on the Ni(1 0 0) surface. For the (1 1 1) surfaces, the value follows the trend of Pt–Ni–Pt(1 1 1) < Pt(1 1 1) < Ni(1 1 1) < Ni–Pt–Pt(1 1 1), which is consistent with experimental observations over these surfaces [13]. On the (1 0 0) surfaces, however, the trend in HBE is different, with the Ni–Pt–Pt(1 0 0) surface binding most weakly among the four surfaces. The DFT results suggest that the presence of a surface Ni monolayer on Pt(1 0 0) reduces the binding energy of atomic hydrogen, in contrast to the increase in HBE upon the deposition of monolayer Ni on Pt(1 1 1).

The binding energy of cyclohexene also shows different trends between the (1 1 1) and (1 0 0) surfaces. The trend is Pt–Ni–Pt(1 1 1) < Pt(1 1 1) < Ni–Pt–Pt(1 1 1), similar to that observed for HBE on these surfaces. In contrast, both subsurface Pt–Ni–Pt(1 0 0) and surface Ni–Pt–Pt(1 0 0) structures show significantly lower binding energies than that on Pt(1 0 0).

Overall, the DFT results in Table 1 indicate that three bimetallic surfaces, Ni–Pt–Pt(1 0 0), Pt–Ni–Pt(1 1 1), and Pt–Ni–Pt(1 0 0), have weaker binding energies than unmodified Pt surfaces for both atomic hydrogen and cyclohexene. Based on the previously reported correlation between binding energies and hydrogenation activity, these three facets on polycrystalline Pt foil should show the unique low-temperature hydrogenation pathway for cyclohexene. The remainder of this paper will provide experimental verification of the adsorption of atomic hydrogen and the hydrogenation of cyclohexene on these bimetallic facets.

4.2. TPD measurements of hydrogen adsorption and desorption

TPD experiments (Fig. 1) are performed on the polycrystalline surfaces to verify the trends predicted by DFT. Previously, it was determined that hydrogen desorbs from Pt(1 1 1) as a relatively broad peak centered near 285 K [14]. Based on this observation, the hydrogen desorption peak at 302 K is attributed to desorption from the (1 1 1) facets of the Pt foil. The hydrogen desorption peak at 354 K is attributed both to Pt(1 0 0) facets, which are predicted by DFT to bind to atomic hydrogen more strongly than Pt(1 1 1) (Table 1), and to step edges and defect sites, which should also have stronger binding energy than Pt(1 1 1) due to the fact that they are under-coordinated. The origins of the low-temperature peak at 228 K and the shoulder at 170 K are not as clear. A similar low-temperature peak is seen on Ni(1 1 1), which was determined to be due to the presence of subsurface hydrogen [26]. It is noted that this low-temperature feature was not seen on Pt(1 1 1) [14], but it is possible that the presence of edges, defect sites, and other low index planes can lead to more facile diffusion of hydrogen

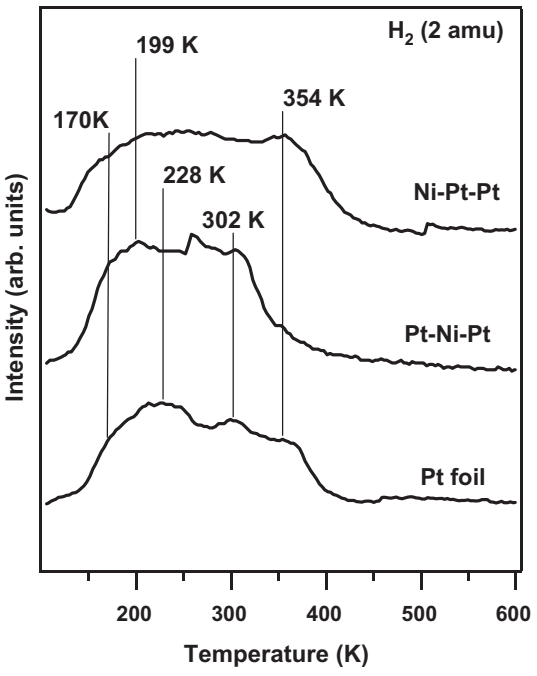

Fig. 1. TPD results following hydrogen adsorption on Ni-modified Pt foil surfaces.

atoms into the subsurface region of the polycrystalline Pt surface [27]. In addition to the possibility of subsurface hydrogen, TPD experiments on Pt(1 0 0)-"hex" have shown desorption of hydrogen from the surface at low temperatures [28].

Upon modification of the Pt foil by depositing one ML surface Ni at 300 K (Ni–Pt–Pt foil), the desorption of hydrogen occurs as one very broad peak. The broadening of the desorption peak in comparison with that from unmodified Pt foil is explained by several simultaneously occurring phenomena. DFT results in Table 1 and previous TPD studies on Ni/Pt(1 1 1) [14] demonstrate that the Ni–Pt–Pt(1 1 1) facets show a higher HBE than Pt(1 1 1), which should lead to an upward shift of the 302 K peak from the unmodified Pt foil. At the same time, DFT results predict that Ni–Pt–Pt(1 0 0) facets have a lower HBE than Pt(1 0 0), as shown in Table 1, which should result in a downward shift in hydrogen desorption temperature for the (1 0 0) facets. In addition, on a vicinal Pt(1 1 1) surface, it was found that Ni can exchange with Pt at step edges at temperatures as low as 150 K [29], and that an ordered surface alloy forms on the terraces at 300 K [29]. Thus, Ni deposition onto Pt foil can result in alloy formation at lower temperatures in comparison with Pt(1 1 1), especially at defect sites and step edges. This makes it likely that the Ni/Pt foil at 300 K is comprised of not only Ni–Pt–Pt(1 1 1) and Ni–Pt–Pt(1 0 0) facets, but also an array of Pt–Ni alloy sites which should lead to a variety of unique binding sites for hydrogen, which should further contribute to the broadening of the TPD peaks.

By heating the Ni–Pt–Pt foil surface to 725 K, the Ni (849 eV)/Pt (241 eV) AES peak-to-peak ratio decreased from ~1.7 to 1.0 due to the diffusion of Ni into the subsurface region of the Pt substrate [19]. The most noticeable difference in the TPD spectrum is the disappearance of the 354 K peak, suggesting the disappearance of any Ni–Pt–Pt(1 1 1) facets and all of the higher energy lattices, step edges, and defect sites responsible for the high temperature peak on unmodified Pt foil. Because the calculated HBE values on

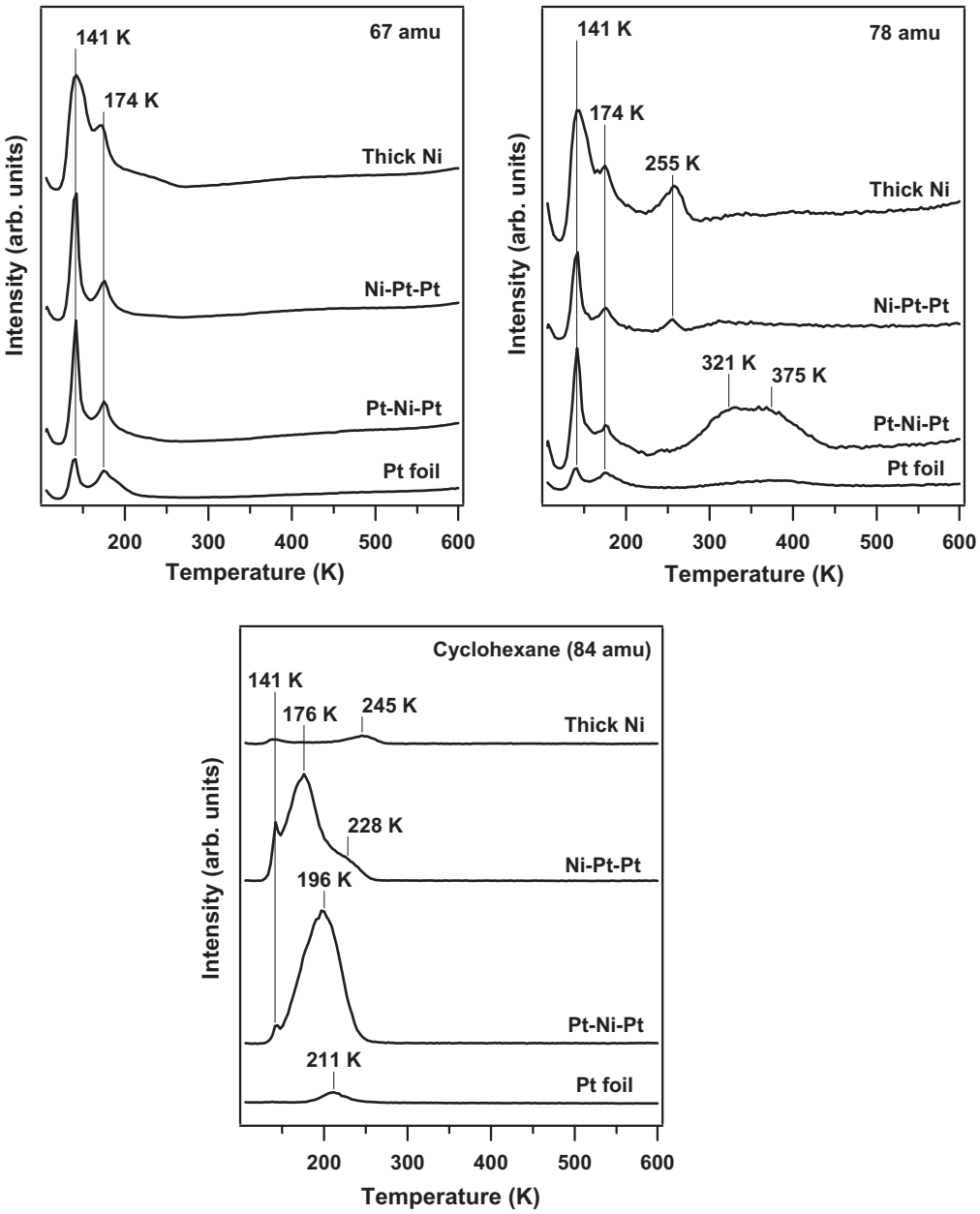

Fig. 2. TPD results following hydrogen and cyclohexene adsorption on Ni-modified Pt foil surfaces.

Pt–Ni–Pt(1 0 0) and Ni–Pt–Pt(1 0 0) are similar, it cannot be determined which of the two sites is present on the surface, though it is expected that Ni should diffuse into Pt(1 0 0) facets as it does in Pt(1 1 1). In summary, all three surfaces in Fig. 1 show some low-temperature desorption states that are not present on single crystal Pt(1 1 1). The next question to be addressed is whether the presence of weakly bonded hydrogen should lead to the low-temperature hydrogenation of cyclohexene from all three surfaces, as described below.

4.3. TPD and HREELS studies of cyclohexene hydrogenation

In previous studies, the reaction cyclohexene was used as a probe reaction to compare the different properties of Pt(1 1 1), surface Ni–Pt–Pt(1 1 1), and subsurface Pt–Ni–Pt(1 1 1) [14]. Cyclohexene binds strongly on Ni–Pt–Pt(1 1 1), leading to complete decomposition without producing gas-phase benzene or cyclohexane. In contrast, both atomic hydrogen and cyclohexene bind more weakly on Pt–Ni–Pt(1 1 1), resulting in a hydrogenation pathway for the production of gas-phase cyclohexane. TPD and HREELS experiments were performed to determine whether similar reaction pathways occur on the more complex polycrystalline bimetallic surface structures. The TPD results presented in Fig. 2 will be discussed first in order to quantify the product yields, and also to gain insights into which adsorbates and intermediates may be present on the surfaces in the HREELS experiments. On a clean Pt foil, the primary reaction pathway is decomposition, as evidenced by a post-TPD C (275 eV)/Pt (241 eV) AES peak-to-peak ratio of 0.76, which is indicative of a surface almost entirely covered with carbon. There are also minor pathways leading to the formation of very small amounts of benzene and cyclohexane, as shown in Fig. 2 and quantified in Table 2.

Modification of Pt foil with 1 ML of Ni results in a significant change in the reaction pathways, with the most obvious difference being a large yield of cyclohexane from both the Pt–Ni–Pt and Ni–Pt–Pt polycrystalline surfaces. The observation of hydrogenation activity on the Ni–Pt–Pt foil is unique to the polycrystalline surface, as single crystal Ni–Pt–Pt(1 1 1) does not exhibit the hydrogenation pathway [14]. This difference suggests that the Ni–Pt–Pt(1 0 0) facets on polycrystalline Pt, and possibly even the Ni-modified step edge and defect sites, are active for cyclohexene hydrogenation. This is not surprising considering the relatively weak cyclohexene binding energy on Ni–Pt–Pt(1 0 0) predicted by DFT (Table 1), and also considering the presence of low-temperature desorption states of hydrogen from the Ni–Pt–Pt foil (Fig. 1).

The amount of gas-phase cyclohexane is quantified by comparing the TPD peak area from the polycrystalline surface to that from single crystal Pt–Ni–Pt(1 1 1), which was estimated to be 0.749 μmol/m^2 based on the amount of cyclohexane molecules desorbing from the single crystal surface [14] and by assuming that the number of surface metal sites is 1.5×10^{15} atoms/cm^2 on Pt(1 1 1). By annealing the Ni–Pt–Pt foil surface to 725 K, the cyclohexane yield increased from 0.754 to 0.997 μmol/m^2. This increase in activity is likely a result of the Ni–Pt–Pt(1 1 1) facets being transformed into the Pt–Ni–Pt(1 1 1) facets on the polycrystalline foil, which should lead to higher hydrogenation yield.

Table 2
Cyclohexene and benzene activity (μmol/m^2).

	Benzene	Cyclohexane
Pt–Ni–Pt(1 1 1)	0.77	0.75
Pt foil	0.02	0.05
Pt–Ni–Pt foil	0.13	0.99
Ni–Pt–Pt foil	0.02	0.75
Thick Ni/Pt foil	0.03	0.04

The main difference between the surface Ni–Pt–Pt foil and subsurface Pt–Ni–Pt foil is that only the latter produces a significant amount of benzene. Thus, while the Ni–Pt–Pt(1 0 0) facets promote hydrogenation, they do not possess favorable binding characteristics to facilitate benzene formation, as confirmed below in the HREELS measurements. In addition to hydrogenation and dehydrogenation reactions, there is evidence of carbonaceous species remaining after the TPD experiments on both Ni–Pt–Pt foil and Pt–Ni–Pt foil, as evidenced by a substantial signal from C in the post-TPD AES measurements. While the relative intensity of this carbon signal is likely a function of the coverage of these carbonaceous species, it cannot be used to accurately quantify the decomposition pathway. Due to alloying, diffusion, segregation, and other mechanisms involving the movement of Pt and Ni relative to each other during a TPD experiment, there is a great deal of uncertainty in the ratio of C/Pt or C/Ni associated with a given coverage of C_xH_y fragments. For this reason, these AES ratios are not used to quantify the amount of carbon species after the TPD experiments on the Ni/Pt polycrystalline surfaces.

As an approximation to a pure Ni metal surface, the hydrogenation activity of a thick Ni film on the Pt foil is also studied as a reference. This surface promotes similar reactions as does the unmodified Pt foil surface. Specifically, there is a relatively high activity toward decomposition, with only minimal activity toward gas-phase benzene or cyclohexane formation. This is not surprising as previous work has shown similar hydrogen and cyclohexene binding energies on Pt(1 1 1) and Ni(1 1 1) [14].

The findings from the TPD results are consistent with the HREEL results in Figs. 3 and 4, which were recorded after the adsorption of cyclohexene on hydrogen pre-dosed surfaces of Pt, Pt–Ni–Pt and Ni–Pt–Pt polycrystalline surfaces. The development of vibrational features on the Pt foil (Fig. 3) is similar to that observed previously on the thermal behavior of cyclohexene on Pt(1 1 1) [9]. At 100 K, the vibrational features are relatively weak, most likely due to random orientations of cyclohexene on the polycrystalline substrate.

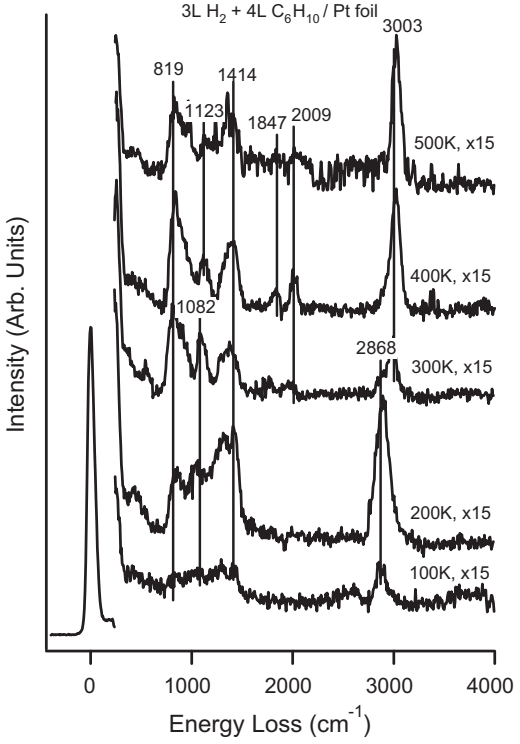

Fig. 3. HREELS of cyclohexene on hydrogen pre-dosed Pt foil after heating to different temperatures.

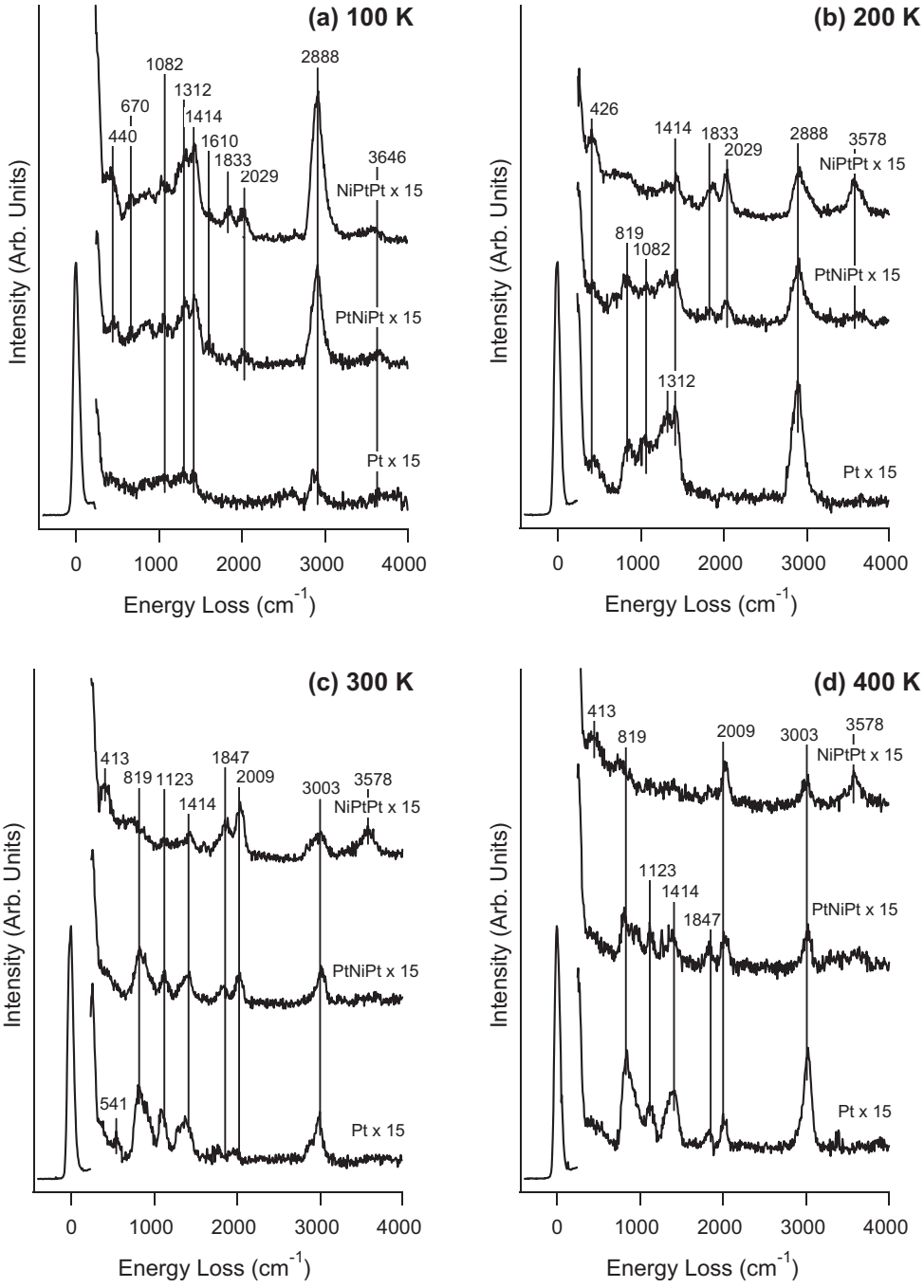

Fig. 4. Comparison of HREELS of cyclohexene on hydrogen pre-dosed Pt and Ni/Pt surfaces after heating to different temperatures.

After heating to 200 K, the vibrational frequencies are characteristic of di-σ-bonded cyclohexene, as summarized in the vibrational assignment in Table 3. The main vibrational features are related to the following modes of cyclohexene, ν(CC) at 819 cm^{-1}, ν(C—C) + $\rho(CH_2)$ at 1082 cm^{-1}, $\omega(CH_2)$ wag at 1312 cm^{-1}, $\omega(CH_2)$ scissor at 1414 cm^{-1}, and ν(—C—H) at 2868 cm^{-1}. The absence of the ν(C=C) and ν(=C—H) modes suggests that cyclohexene is di-σ-bonded through the C=C bond on the Pt foil. After heating to 300 K, the spectrum is consistent with a mixture of adsorbed cyclohexene and benzene. After heating to 400 K, the spectrum is characteristic of chemisorbed benzene with the following vibrational modes [9], ν(C—C) at 819 cm^{-1}, δ(C—H) at 1123 cm^{-1}, ν(C—C) + δ(C—C) at 1414 cm^{-1}, and ν(C—H) at 3003 cm^{-1}. The intensities of the ν(C—C) at 819 cm^{-1} and ν(C—H) at 1123 cm^{-1} modes start to decrease after heating to 500 K, indicating that adsorbed benzene starts to undergo either decomposition or desorption. The near absence of gas-phase benzene in the TPD measurements (Fig. 2) indicates that the benzene intermediate on the Pt foil undergoes dissociation instead of desorption.

Fig. 4 compares HREELS results on Ni–Pt–Pt and Pt–Ni–Pt foil surfaces after heating the adsorbed layers to different temperatures. The corresponding HREEL spectra from unmodified Pt foil were also included to provide a point of comparison. Using similar vibrational assignment in Table 3, the 100 K HREEL spectra on the subsurface Pt–Ni–Pt and surface Ni–Pt–Pt foils are consistent with the adsorption of di-σ-bonded cyclohexene. A closer inspection also reveals the presence of relatively weak features at ~670 and ~1610 cm^{-1}. In previous studies following the adsorption of

Table 3
Vibrational assignments for adsorbed species on Pt foil and Ni-modified Pt foil substrates.

Cyclohexene HREELS assignments, frequency (cm^{-1})				
Mode	Liquid	Pt	PtNiPt	NiPtPt
Ring deformation	175, 280, 393, 452	–	–	–
ν(M—C)	–	426, 541	440	413
Skeletal distortion	640, 670	–	–	–
δ(C═C)	720	–	670	670
ν(C—C)	810, 905, 917	819	812	751
ν(C—C) + $\rho(CH_2)$	1038	1082	1055	1035
$\omega(CH_2)$ rock	1138	1123	1123	1099
$\omega(CH_2)$ twist	1241, 1264	–	–	–
$\omega(CH_2)$ wag	1321–1350	1312	1312	–
$\omega(CH_2)$ scissors	1438–1456	1414	1427	1427
ν(C═C)	1653	–	1610	1603
ν(CO)	–	1847, 2009	1833, 2029	1860, 2029
ν(—C—H)	2840–2993	2888, 3003	2902, 3024	2916, 3010
ν(═C—H)	3026, 3065	–	–	3078
ν(OH)[a]		–	3646	3578

[a] Features near 3600 cm^{-1} are due to surface hydroxyl species from the dissociative adsorption of water.

cyclohexene on single crystal Pt–Ni–Pt(1 1 1), these two features were much better resolved and were assigned to the δ(C═C) and υ(C═C) modes, respectively, of weakly σ-bonded cyclohexene with the C═C bond parallel to the single crystal surface [9]. The presence of weakly bonded cyclohexene on Pt–Ni–Pt(1 1 1) is consistent with the DFT prediction (Table 1) and is responsible for the low-temperature hydrogenation pathway. Using a similar argument, the presence of these two features in the current study suggests that weakly σ-bonded cyclohexene should also be present on the Pt–Ni–Pt and Ni–Pt–Pt polycrystalline surfaces, although their relative intensities are not as intense as those on the single crystal surfaces, likely due to the lack of preferred orientation of the C═C bond on the polycrystalline foil. The disappearance of these two features at 200 K is consistent with the TPD detection of gas-phase cyclohexane at 176 K from Ni–Pt–Pt and at 196 K from Pt–Ni–Pt (Fig. 2). At 200 K and higher temperatures, the HREEL spectra on the Pt–Ni–Pt foil are qualitatively similar to those on unmodified Pt foil, with the surface species being mainly di-σ-bonded cyclohexene at 200 K and chemisorbed benzene at higher temperatures. One noticeable difference is that the benzene features are less intense on Pt–Ni–Pt than on Pt, consistent with the TPD results (Fig. 2) that a significant amount of benzene desorbs from the Pt–Ni–Pt foil instead of remaining on the surface and undergoing subsequent decomposition. In comparison, one of the characteristic features for benzene, ν(C—C) at 819 cm^{-1}, is not well developed on the Ni–Pt–Pt surface at any temperature. This observation is consistent with the near absence of gas-phase benzene from this surface (Fig. 2), suggesting that the decomposition of cyclohexene on Ni–Pt–Pt does not occur through a stable benzene intermediate.

4.4. Similarities and differences between Ni/Pt(1 1 1) and Ni/Pt foil

The most significant similarity between the single crystal and the polycrystalline surfaces is the observation of hydrogenation pathway on the subsurface Pt–Ni–Pt structures. As predicted in the DFT calculations in Table 1, both the Pt–Ni–Pt(1 1 1) and Pt–Ni–Pt(1 0 0) facets should bond to atomic hydrogen and cyclohexene weakly, resulting in the low-temperature hydrogenation pathway (Fig. 2) that is not present on either polycrystalline Pt or the thick Ni film. Recent DFT calculations [30] indicate that the subsurface Pt–Ni–Pt structure is thermodynamically preferred under reducing conditions and in the presence of adsorbed hydrogen. This is confirmed experimentally using *in situ* X-ray absorption near edge spectroscopy (XANES) measurements of ML Ni on polycrystalline Pt, where the surface and subsurface structures can be recycled using oxidation–reduction treatment, with the subsurface Pt–Ni–Pt being the preferred structure under atmospheric pressure of hydrogen [31] These results suggest that the desirable Pt–Ni–Pt subsurface structure should also be present in supported Ni/Pt bimetallic catalysts under hydrogenation conditions. This is consistent with the recent batch and flow reactor studies of hydrogenation of cyclohexene on Ni/Pt bimetallic catalysts supported on γ-Al_2O_3, which show significantly higher hydrogenation activity than supported Ni and Pt monometallic catalysts [32].

One interesting difference between the single crystal and the polycrystalline surfaces is the detection of the hydrogenation pathway on polycrystalline Ni–Pt–Pt, which is not present on the single crystal Ni–Pt–Pt(1 1 1) [14]. Based on the DFT predictions in Table 1 and the TPD results, this difference is most likely related to the presence of the Ni–Pt–Pt(1 0 0) facets on the polycrystalline foil. Both atomic hydrogen and cyclohexene are predicted to adsorb weakly on Ni–Pt–Pt(1 0 0), and this is likely responsible for of the hydrogenation pathway on the polycrystalline Ni–Pt–Pt surface. It is also important to point out that, although weakly adsorbed hydrogen is detected in TPD on polycrystalline Pt, this surface does not show the hydrogenation pathway due to the fact that cyclohexene binds strongly on this surface. This observation further confirms previous conclusions that atomic hydrogen and alkenes both need to be weakly bonded in order to achieve the low-temperature hydrogenation [3].

Finally, another difference is in the relative yields of gas-phase cyclohexane and benzene. As shown in the TPD yield in Table 3, on single crystal Pt–Ni–Pt(1 1 1) the yields of cyclohexane and benzene are comparable. In contrast, on polycrystalline Pt–Ni–Pt the yield of benzene (0.13 μmol/m^2) is significantly lower than cyclohexene (0.997 μmol/m^2), although benzene is detected as a reaction intermediate in the HREELS measurements (Fig. 4). This difference is most likely due to the presence of the (1 0 0) facets and defect sites on the polycrystalline foil, which promote the decomposition of the benzene intermediate instead of desorption from the surface.

5. Conclusions

The results in the current paper demonstrate general similarities and interesting differences between single crystal and polycrystalline Ni/Pt bimetallic surfaces. Similar to the single crystal Pt–Ni–Pt(1 1 1) subsurface structure, the Pt–Ni–Pt foil is active for the low-temperature hydrogenation due to the presence of weakly bonded atomic hydrogen and cyclohexene. However, unlike Ni–Pt–Pt(1 1 1), the Ni–Pt–Pt foil is also active toward the hydrogenation, most likely related to the DFT prediction and

experimental verification that the Ni–Pt–Pt(1 0 0) portion of the polycrystalline bimetallic foil also bonds to hydrogen and cyclohexene more weakly than unmodified Pt. Thus, it is expected that supported Ni/Pt bimetallic catalysts, which should consist of Pt–Ni–Pt(1 1 1), Pt–Ni–Pt(1 0 0), and possibly Ni–Pt–Pt(1 0 0) facets, should also exhibit enhanced low-temperature hydrogenation properties, as reported recently in reactor studies on supported Ni/Pt bimetallic catalysts on γ-Al_2O_3 [32]. The correlation between single crystal, polycrystalline, and supported bimetallic catalysts demonstrates that DFT calculations and UHV studies on single crystal surfaces should provide useful guidance in selecting novel bimetallic catalytic materials for hydrogenation reactions.

Acknowledgment

This work was supported by the Department of Energy, Office of Basic Energy Sciences (DOE/BES Grant No. DE-FG02-00ER15104).

References

[1] J.H. Sinfelt, Account Chem. Res. 10 (1977) 15.
[2] C.A. Menning, J.G. Chen, Topics Catal. 53 (2010) 338.
[3] J.G. Chen, C.A. Menning, M.B. Zellner, Surf. Sci. Rep. 63 (2008) 201.
[4] J.A. Rodriguez, D.W. Goodman, Science 257 (1992) 897.
[5] B. Hammer, J.K. Norskov, Adv. Catal. 45 (2000) 71.
[6] M. Neurock, R.A. van Santen, J. Phys. Chem. B 104 (2000) 11127.
[7] D.W. Goodman, Ultramicroscopy 34 (1990) 1.
[8] V. Pallassana, M. Neurock, J. Catal. 191 (2000) 301.
[9] H.H. Hwu, J. Eng Jr., J.G. Chen, J. Am. Chem. Soc. 124 (2002) 702.
[10] N.A. Khan, H.H. Hwu, J.G. Chen, J. Catal. 205 (2002) 259.
[11] O. Skoplyak, M.A. Barteau, J.G. Chen, J. Phys. Chem. B 110 (2006) 1686.
[12] L.E. Murillo, A.M. Goda, J.G. Chen, J. Am. Chem. Soc. 129 (2007) 7101.
[13] J.R. Kitchin, N.A. Khan, M.A. Barteau, J.G. Chen, B. Yakshinksiy, T.E. Madey, Surf. Sci. 544 (2003) 295.
[14] M.P. Humbert, J.G. Chen, J. Catal. 257 (2008) 297.
[15] M.P. Humbert, L.E. Murillo, J.G. Chen, ChemPhysChem 9 (2008) 1262.
[16] A.L. Stottlemyer, H. Ren, J.G. Chen, Surf. Sci. 603 (2009) 2630.
[17] N. McMillan, C. Snively, J. Lauterbach, Surf. Sci. 601 (2007) 772.
[18] P.J. Cumpson, M.P. Seah, Surf. Interface Anal. 25 (1997) 430.
[19] C.A. Menning, J.G. Chen, J. Chem. Phys. 128 (2008) 164703.
[20] D.A. Hansgen, D.G. Vlachos, J.G. Chen, Nat. Chem. 2 (2010) 484.
[21] K. Christmann, Surf. Sci. Rep. 9 (1988) 1.
[22] K.E. Lu, R.R. Rye, Surf. Sci. 45 (1974) 677.
[23] D.M. Collins, W.E. Spicer, Surf. Sci. 69 (1977) 85.
[24] R.W. McCabe, L.D. Schmidt, Surf. Sci. 65 (1977) 189.
[25] N.M. Markovic, P.N. Ross, Surf. Sci. Rep. 45 (2002) 121.
[26] A.D. Johnson, K.J. Maynard, S.P. Daley, Q.Y. Yang, S.T. Ceyer, Phys. Rev. Lett. 67 (1991) 927.
[27] J. Greeley, W.P. Krekelberg, M. Mavrikakis, Angew. Chem. Int. Ed. 43 (2004) 4296.
[28] S.J. Dixon-Warren, A.T. Pasteur, D.A. King, J. Chem. Phys. 103 (1995) 2261.
[29] P. Gambardella, K. Kern, Surf. Sci. 475 (2001) L229.
[30] C.A. Menning, J.G. Chen, J. Chem. Phys. 130 (2009) 174709.
[31] C.A. Menning, J.G. Chen, J. Power Sources 195 (2010) 3140.
[32] S. Lu, W.W. Lonergan, J.P. Bosco, S. Wang, Y. Zhu, Y. Xie, J.G. Chen, J. Catal. 259 (2008) 260.